

## Research Article

# La Loaded TiO<sub>2</sub> Encapsulated Zeolite Y Catalysts: Investigating the Characterization and Decolorization Process of Amaranth Dye

Atheel Hassan Alwash,<sup>1,2</sup> Ahmad Zuhairi Abdullah,<sup>1</sup> and Norli Ismail<sup>3</sup>

<sup>1</sup> School of Chemical Engineering, Universiti Sains Malaysia, 14300 Nibong Tebal, Penang, Malaysia

<sup>2</sup> Department of Chemistry, College of Science, Al-Nahrain University, Al-Jadiriya, Baghdad, Iraq

<sup>3</sup> School of Industrial Technology, Universiti Sains Malaysia, 11800 Nibong Tebal, Penang, Malaysia

Correspondence should be addressed to Atheel Hassan Alwash; [atheel\\_eng78@yahoo.com](mailto:atheel_eng78@yahoo.com)

Received 26 January 2013; Revised 2 June 2013; Accepted 10 June 2013

Academic Editor: Jose M. Guisan

Copyright © 2013 Atheel Hassan Alwash et al. This is an open access article distributed under the Creative Commons Attribution License, which permits unrestricted use, distribution, and reproduction in any medium, provided the original work is properly cited.

Lanthanide ions loaded TiO<sub>2</sub> encapsulated into Y zeolite catalysts were synthesized and used in sonocatalytic degradation of Amaranth dye in aqueous solution. The support zeolite Y was modified by different loading of Ti and La species using ion exchange method. The sonocatalytic reaction condition was carried out at 10 mg/L initial dye concentration, original pH, 1.5 g/L of catalyst loading with low ultrasonic frequency of 40 KHz. Different characterization techniques were used to reveal the physicochemical characteristics of the catalysts. Successful loading of TiO<sub>2</sub> and La/TiO<sub>2</sub> into zeolite Y was achieved. The framework of zeolite Y remained unchanged after the loading of TiO<sub>2</sub>. Titanium species was bound to the framework of zeolite through Ti–O–Si bonds through isomorphous substitution of Si in the zeolite. The ultrasonic degradation of Amaranth dye was enhanced by the TiO<sub>2</sub> encapsulation with a maximum degradation efficiency of 50% after 120 min of reaction. However, the activity of the catalyst decreased after the loading of lanthanum. This decrease was attributed to the poor contact between the metal crystallites located on the external surface and the titanium encapsulated into cages of zeolite Y.

## 1. Introduction

Titanium dioxide is generally considered to be a very efficient photo- or sonocatalyst that is nontoxic, stable, and cheap [1]. It exhibits high durability, corrosion resistance, and high oxidation potential of the valence band that ensures its general applicability to a wide range of substrates [2]. On the other hand, fast charge carrier recombination, low interfacial charge-transfer rates, and recycling difficulties were the main drawbacks of using bare TiO<sub>2</sub> [3]. In order to overcome these problems, two methods have been suggested to increase its activity. The first one is through doping of the transition metal ions into titanium dioxide to suppress the recombination of electrons holes. Song et al. [4], Jamalluddin and Abdullah [5], Wang et al. [6], and many other researches have reported the differences in the catalytic activity of titanium oxide with different types of doping metals. Secondly, loading of titanium dioxide onto suitable supports could reduce the problem of

catalyst separation after the reaction. Loading of TiO<sub>2</sub> nanoparticles on porous supports has been attempted using activated carbon [7, 8], fiber glass [9], clay [10], and zeolites [11] as the support materials.

Zeolites are good adsorbents and eco-friendly materials possessing high surface area and high thermal stability. Additionally, these materials possess amphoteric properties such as Lewis acidity (denotes electron-accepting ability) and Lewis basicity (describes their electron-donating property) [12, 13]. The nature of modification depends mainly on the specific zeolite structure, framework composition, nature of cation, and pore structure. The behavior of the catalyst and its practical applications will be influenced by the properties of the zeolites such as particle size, surface area, pore diameter, mechanical strength, microbial resistance, thermal stability, chemical durability, hydrophobic/hydrophilic character, ease of regeneration, loading capacity, and cost [14].

The possibility for titanium encapsulation into the pores of zeolite is interesting as far as catalysis is concerned due to the high internal surface area of zeolite. Titanium encapsulation into zeolite has been recently investigated for its use in photocatalytic reaction [15]. Chen et al. [16], Liu et al. [15], and Zhang et al. [17] have reported the characterization and the photocatalytic activity of titanium encapsulated into the pores of zeolite for the degradation of different organic compounds while a certain degree of success has been reported.

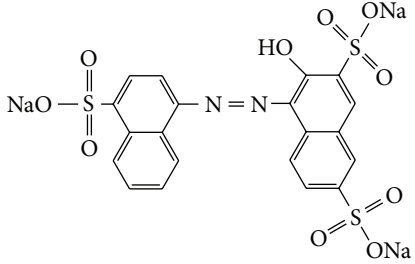
It is well known that the  $\text{TiO}_2$  is irradiated by the absorption of the UV light generated from the ultrasonic process that is 375 nm leading to high oxidation potential and the generation of  $e^- - h^+$  pair. This fact is similar to the photocatalytic process. However, the use of ultrasound as an irradiation source for the heterogeneous catalysts instead of photocatalytic process can be useful in many aspects such as the higher penetrating depths of ultrasonic up to 20–30 cm which is the superior characteristic of ultrasonication process compared to the low penetrability during the photocatalytic process in water medium (limited to several millimeters), improvement in the diffusion of reactant from the bulk solution to the surface of catalyst, continuous cleaning of the catalyst surface which is ascribed to the desorption of the generated product during oscillation. In addition, ultrasonic process prevents the aggregation of the catalyst particles due to the fragmentation of the particles into smaller sizes thus increasing the active surface area available for the reaction [18]. Therefore, it is of great interest to investigate the use of similar material in sonocatalytic reaction since this process does not have the problems of low light penetration, long reaction time, or the need for specific system design.

In this study,  $\text{La}^{3+}$  has been loaded onto the encapsulated  $\text{TiO}_2$  on the hypothesis that the presence of dopant can retard the recombination between  $e^- - h^+$  pair generated from the irradiated  $\text{TiO}_2$  nanoparticles encapsulated into zeolite to consequently improve the catalytic activity [17]. The coincorporation of both La and Ti into the framework of zeolite will give the chance to occupy most of the internal and external surface areas of zeolite with active metals thus enhancing the catalytic activity. As such, specific characteristics and sonocatalytic behaviors of encapsulated  $\text{TiO}_2$  into zeolite Y with and without the presence of lanthanum dopant have been elucidated to investigate the ability of the catalyst to degrade Amaranth dye as a probe substance in this work. Amaranth is an ionic azo dye with three sulfonic groups in its structures usually; it is used for dyeing the fibers, wool, and textile printing silk as well as photography.

## 2. Experimental

**2.1. Materials.** H-Y zeolite with Si/Al ratio of 15 was obtained from Zeolyst International. Amaranth dye, potassium titanoxalate dehydrate (99%), and sodium chloride bioxtra (99.5%) were obtained from Sigma-Aldrich, while lanthanum nitrate III hexahydrate (99.999%) was obtained from Aldrich. The important properties of the dye molecules are given in Table 1. Distilled deionized water was obtained by purifying distilled water with an Elga-Pure Water Purification

TABLE 1: Molecular structure and properties of Amaranth dye.

Properties	Info
Molecular structure	
Other names	Acid red 27, FD&C Red 2, Food Red 9
Molecular weight	604.47 $\text{gmol}^{-1}$
Stability	Soluble in water
C.I.	16185
$\lambda_{\text{max}}$	521 nm

(UHQ W) system. It was used in the preparation of dye solutions used in the study.

### 2.2. Catalyst Preparation Method

**2.2.1. Preparation of Na-Y Zeolite.** The dried H-Y zeolite was first converted to its sodium form by means of an ion exchange method [19]. The material was washed with 1 M NaCl at 80°C for 4 h in such a way that the ratio of zeolite Y to sodium chloride solution was 1 : 80. The slurry was then filtered and washed with distilled deionized water to remove excess NaCl. In order to get a sufficient exchange of sodium with the zeolite, the previous procedure was repeated twice. The sample was then dried overnight at a temperature of 80°C and then calcined in a muffle furnace at 550°C for 5 h.

**2.2.2. Introduction of  $\text{TiO}_2$  into Na-Y Zeolite.** Several samples of Na-Y zeolite incorporated with  $\text{TiO}_2$  were prepared using the procedure reported by Liu et al. [15]. Different concentrations of potassium titanoxalate (from 0.56–2.82  $\times 10^{-2}$  mol/L) were dissolved in 100 mL of distilled deionized water. Then, 1.0 g of support (Na-Y zeolite) was added to each solution and they were kept under continuous stirring for 12 h to allow ion-exchange process. After the ion exchange step, the catalysts were filtered with a membrane filter (pore size 0.45  $\mu\text{m}$ ) and washed with excessive amount of water to avoid the physically adsorbed titanium species from aggregating on the external surface of the zeolite. Then, the catalysts were dried overnight in an oven at 100°C. The previous procedure was repeated to get higher loading of titanium and the catalysts were denoted as  $\text{Ti}_1\text{-NaY}$ ,  $\text{Ti}_2\text{-NaY}$ ,  $\text{Ti}_3\text{-NaY}$ , and  $\text{Ti}_4\text{-NaY}$  according to the increasing titanium content in catalyst. Next, the catalysts were calcined in a furnace at 550°C for 5 h with a ramping rate of 5°C/min. Prior their use in the reaction, the catalysts were ground into fine powder and kept in dry cabinet.

In order to investigate the effect of metal loading on the activity of the catalyst, different concentrations of lanthanum

nitrate solution were dissolved in 100 mL of distilled deionized water and 1 g of  $\text{Ti}_4\text{-NaY}$  was added to each solution, and they were kept under continuous stirring for 12 h at ambient temperature. Then, the catalysts were filtered with a membrane filter (pore size  $0.45\ \mu\text{m}$ ) and washed. This procedure was repeated to get higher loading of La in the catalyst [20]. After drying overnight at  $100^\circ\text{C}$  and calcinations at  $550^\circ\text{C}$  for 5 h, the catalysts were ground and kept in a dry cabinet. The final catalysts are denoted as 0.32% La/ $\text{Ti}_4\text{-NaY}$ , 0.64% La/ $\text{Ti}_4\text{-NaY}$ , and 1.28% La/ $\text{Ti}_4\text{-NaY}$  using the actual Wt% of La ions which was checked by the ICP technique.

**2.3. Characterization Technique.** Physicochemical characterizations of the catalysts with different analytical techniques were performed on the most potential catalysts. The loadings of titanium and lanthanum after the ion exchange process were checked by means of an inductively coupled plasma ICP-MS spectrometer. Meanwhile, X-ray diffraction patterns of the catalyst samples were determined using an XRD system (Philips Goniometer PW 1820). Surface analysis was also performed using nitrogen adsorption/desorption (Micromeritics ASAP 2020) based on  $\text{N}_2$  adsorption process at 77 K. The energy dispersive X-ray analysis (EDAX) system from (Oxford INCA/ENERGY-350) was also used to analyse the type of metals at the catalyst surface. The reflectance of the solid samples was determined using UV-Vis spectrophotometer (Perkin Elmer) in a wavelength range between 190 and 1,100 nm. The FT-IR spectroscopic measurements were carried out using a Perkin-Elmer spectrophotometer in which the spectra were recorded in the range of  $400\text{--}4,000\ \text{cm}^{-1}$  while transmission electron microscope/(TEM) imaging was equipped with an image analyzer and operated at 120 kV. The roughness of the catalyst surface was checked using SPA 400 AFM technique.

**2.4. Sonocatalytic Reaction.** All experiments were carried out in a 250 mL cylindrical vessel and placed in an ultrasonic bath (Cole-Parmer) for up to 2 h. Before the ultrasonic reaction was initiated, the solution was stirred for 30 min at room temperature to maintain the good dispersion of catalyst with the dye solution. The experimental conditions were set at an initial Amaranth dye concentration of 10 mg/L, a catalyst amount of 1.5 g/L, and the solution pH was kept at its original level without any adjustment. The ultrasonic output power was fixed at 50 W with a frequency of 40 kHz. The catalytic activity was measured by calculating the degradation efficiency by means of a UV-Vis spectrophotometer. The performance of the catalysts was evaluated by adding 1.5 g/L of catalyst into the dye solution treated under ultrasonic irradiation. During the reaction, a sample solution was withdrawn at each time interval and centrifuged using a Kubota 5910 centrifuge to separate the supernatant. Then, concentration of the dye solution was determined at a maximum absorbance wavelength of 521 nm. The degradation efficiency of the catalyst was calculated based to the following equation:

$$\text{degradation efficiency (\%)} = \left[ 1 - \left( \frac{C_t}{C_0} \right) \right] \times 100\%, \quad (1)$$

TABLE 2: Elemental composition of the prepared materials.

Catalyst sample	Composition (wt.%)	
	Ti	La
$\text{Ti}_2\text{-NaY}$	0.25	—
$\text{Ti}_4\text{-NaY}$	0.30	—
0.32% La/ $\text{Ti}_4\text{-NaY}$	0.30	0.32
0.64% La/ $\text{Ti}_4\text{-NaY}$	0.30	0.64
1.28% La/ $\text{Ti}_4\text{-NaY}$	0.30	1.28

where  $C_0$  (mg/L) is the initial concentration of dye and  $C_t$  (mg/L) is the concentration of dye at certain reaction time,  $t$  (min).

### 3. Results and Discussions

#### 3.1. Characterization of Catalyst

**3.1.1. ICP Analysis.** The results of ICP analysis for the actual amount of titanium and lanthanum in the zeolite catalysts prepared through ion-exchange method are shown in Table 2. The amount of titanium and lanthanum loaded into zeolite was found to increase with increasing concentration of Ti and La solutions used during the ion-exchange process. This was an expected result as higher concentration would shift the equilibrium in the ion-exchange process towards forward reaction. The highest loading of  $\text{TiO}_2$  was achieved with  $\text{Ti}_4\text{-NaY}$  with a loading of 0.30 wt.%. Meanwhile, the La content in the catalyst was varied between 0.32 and 1.28 wt.%.

**3.1.2. Surface Analysis.** The BET surface area for zeolite (NaY), titanium encapsulated into zeolite ( $\text{Ti}_4\text{-NaY}$ ), and 0.64% La/ $\text{Ti}_4\text{-NaY}$  were obtained by means of  $\text{N}_2$  isotherm surface analyzer. It was observed that the surface area of zeolite was decreased after the encapsulation of  $\text{TiO}_2$  into zeolite from  $771\ \text{m}^2/\text{g}$  for NaY zeolite to  $754\ \text{m}^2/\text{g}$  for  $\text{Ti}_4\text{-NaY}$  with increasing loading of  $\text{TiO}_2$ . This slight reduction in surface area indicated the successful loading of titanium oxide during the repeated ion-exchange method. Severe drop in the surface area did not occur to indicate that pore excessive mouth clogging did not happen even at the highest  $\text{TiO}_2$  loading. This could be due to the general characteristics of zeolite Y internal pores which are relatively large ( $7.4\ \text{\AA}$ ) with a high void fraction of about 48% [21]. However, after the loading of 0.64 wt.% of La into  $\text{Ti}_4\text{-NaY}$ , the surface area of the produced catalyst was decreased to  $618\ \text{m}^2/\text{g}$ .

The pore volume of catalysts was also found to decrease from 0.249 nm for NaY zeolite to 0.242 nm for  $\text{Ti}_4\text{-NaY}$ . This slight reduction was ascribed to the partial agglomeration of the  $\text{TiO}_2$  cluster inside the pores of zeolite after the ion-exchange and calcination steps. Based on the special characteristics of this zeolite that has an external surface area of about 1% of the inner surface area (close to  $6\ \text{m}^2/\text{g}$ ), pore opening of  $7.4\ \text{\AA}$ , and super cages diameter of 1.3 nm, titanium ions could be entrapped within the supercages of zeolite during the ion-exchange process depending on the size of  $\text{TiO}_2$  cluster that formed [21]. It should be noted that potassium titanooxalate

formed a very clear solution due to its high solubility in water and it did not form any colloidal suspension. This high solubility allowed titanium ions to diffuse into the internal cavities of zeolite Y during the ion-exchange process. However, the maximum size of the  $\text{TiO}_2$  cluster presented in the supercages might not be larger than 1.3 nm which is the diameter of the supercage.

For the case of 0.64%  $\text{La}/\text{Ti}_4\text{-NaY}$  the pore volume of the catalyst was reduced to  $0.188 \text{ cm}^3/\text{g}$ . The reduction in pore volume after the loading of La could be ascribed to the partial interaction of these ions with the framework of zeolite. However, it seems that there was an excess amount of La that could not any more enter the formwork of zeolite, and, instead, it was accumulated on the surface of it consequently causing this obvious reduction in surface area of the catalyst as it was mention earlier.

**3.1.3. XRD Analysis.** The crystalline structure of the catalyst particles was determined using X-ray powder diffraction method. The XRD patterns of selected catalysts with different  $\text{TiO}_2$  loadings are shown in Figure 1. The high crystalline from of the parent zeolite (NaY) was very obvious from the diffraction patterns of XRD that exhibited reflections at  $2\theta$  values of 12, 15, 18, 20, 23, 31, and 34 which were typical to the structure of zeolite Y. These results were in agreement with those reported by Tayade et al. [19]. The structure of zeolite remained virtually unchanged after being loaded with titanium oxide ( $\text{Ti}_2\text{-NaY}$  and  $\text{Ti}_4\text{-NaY}$ ) to indicate that the  $\text{TiO}_2$  did not significantly affect the framework structure of the zeolite. However, no new peaks could be detected for anatase at  $2\theta 25.1^\circ$  after  $\text{TiO}_2$  loading into zeolite. This could be due to the low loading of  $\text{TiO}_2$  as it was detected by the ICP technique or the  $\text{TiO}_2$  clusters located within the zeolite pores that were very small leading to unclear diffraction patterns. Furthermore, the location of  $\text{TiO}_2$  clusters within the internal pores could be difficult to be detected under XRD [17]. Chen et al. [16] reported that they did not observe any diffraction peak at low loading of titanium oxide incorporated into zeolite (below  $83 \text{ mg/g}$  of catalyst) since the amount of  $\text{TiO}_2$  was not high enough to give clear diffraction peaks.

The XRD diffraction patterns for  $\text{La}/\text{Ti}_4\text{-NaY}$  at different loading of La are shown in Figure 1. It was clear that there was a reduction in the intensity of the peaks after the loading of small amount of lanthanum. All the peaks that are associated with the crystalline of zeolite were converted to wide and short peaks. Even though the loadings for both  $\text{TiO}_2$  and lanthanum oxide were very small, but the difference in the intensities of the peaks after both loading was significant. The reduction in the intensity of the peaks for the case of La loading can give an indication that the lanthanum oxide mostly covered the surface of the support and, caused this reduction in peaks intensities These results were in good agreement with the results of surface analysis.

Table 3 presents summarized information about the unit cell parameters and the unit cell volume of the NaY support before and after the loading of Ti and La metals. From the results of XRD diffraction, it was observed that the crystal structure was a polyhedral cubic form and it was able to keep

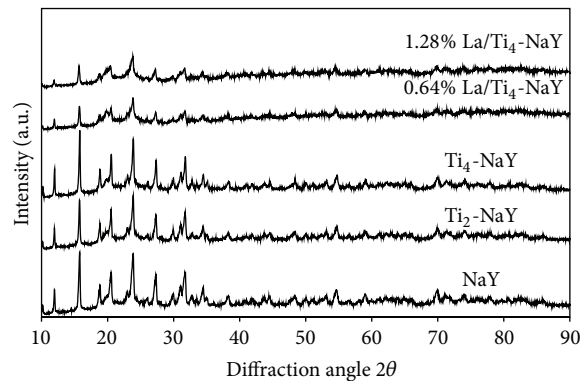


FIGURE 1: X-ray diffraction patterns of various titanium-modified zeolite Y catalysts.

TABLE 3: Unit cell parameters ( $\text{\AA}$ ) and ( $V$ ) crystal volume ( $\text{\AA}^3$ ) of different catalysts.

Catalyst	$a$ ( $\text{\AA}$ )	$b$ ( $\text{\AA}$ )	$c$ ( $\text{\AA}$ )	$(V)$ $\text{\AA}^3$
NaY	24.342	24.342	24.342	14423.43
$\text{Ti}_2\text{-NaY}$	24.322	24.322	24.322	14387.91
$\text{Ti}_4\text{-NaY}$	24.327	24.327	24.327	14396.78
0.64% $\text{La}/\text{Ti}_4\text{-NaY}$	24.342	24.342	24.342	14423.43
1.28% $\text{La}/\text{Ti}_4\text{-NaY}$	24.363	24.363	24.363	14460.79

its original structure even after the ion exchange with both Ti and La species. There was a significant reduction in the unit cell volume of zeolite from  $14423.43 \text{ \AA}^3$  to  $14396.78 \text{ \AA}^3$  after the loading of Ti species. This change was ascribed to the reduction in the unit cell parameter due to the replacement between the Ti and the framework of NaY. Similar result was reported by Zhao et al. [22] and Liu et al. [15]. After the loading of La ions onto  $\text{Ti}_4\text{-NaY}$ , an increase in the volume of the unit cell was observed with increasing loading of La. This increase in the unit cell volume could attribute to the deposition of lanthanum oxide on the surface of  $\text{Ti}_4\text{-NaY}$  to cause some deformation in the crystal lattice of the support.

**3.1.4. FTIR Analysis.** Infrared spectra of the NaY, Ti encapsulated zeolite with two different loadings of La, that is, 0.64%  $\text{La}/\text{Ti}_4\text{-NaY}$  and 1.32%  $\text{La}/\text{Ti}_4\text{-NaY}$ , are shown in Figures 2(a) and 2(b). A new absorption band at a wavelength of  $950 \text{ cm}^{-1}$  appeared and it was attributed to Ti-O-Si bond. This result was in agreement with a reported work by Wang et al. [20]. The peak at  $950 \text{ cm}^{-1}$  was detected for all zeolite catalysts loaded with  $\text{TiO}_2$  and it was ascribed to the replacement of tetrahedral Si with Ti during the ion-exchange method [20]. The intensity was influenced by the amount of  $\text{TiO}_2$  presented on the zeolite support [23].

For NaY, the peak at  $950 \text{ cm}^{-1}$  is attributed to Si-OH bond [24], and from Figure 2(a), it is clear that there is no such peak. Thus, this peak was an indication of successful isomorphous substitution of Ti with Si to produce Si-O-Ti [25]. At  $1,000 \text{ cm}^{-1}$ , a slight shift towards higher frequency attributed

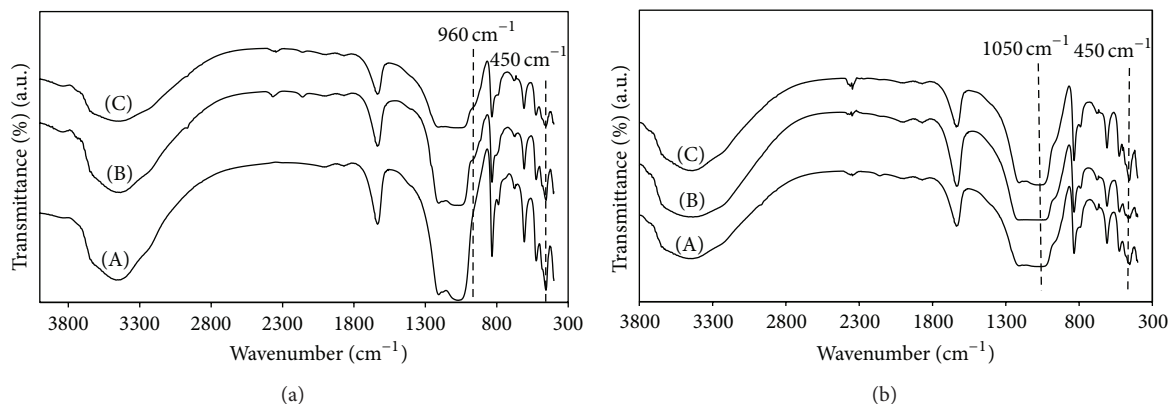


FIGURE 2: (a) FTIR spectra of NaY (A), Ti<sub>2</sub>-NaY (B), and Ti<sub>4</sub>-NaY (C). (b) FTIR spectra of Ti<sub>4</sub>-NaY (A), 0.64% La/Ti<sub>4</sub>-NaY (B), and 1.32% La/Ti<sub>4</sub>-NaY (C).

to the T–O–T or O–T–O (T = Si or Al) stretching vibration of the framework was observed. This observation demonstrated the effect of the Ti species on zeolite framework [26]. Liu et al. [15] reported similar results in their attempt for Ti encapsulation into zeolite Y. The bands detected in the range from 500 to 700 cm<sup>-1</sup> for all the samples were ascribed to pseudolattice vibrations while the bands below 400 cm<sup>-1</sup> were ascribed to the lattice vibration [27]. However, a stretching vibration peak attributed to Ti–O bond was observed at 460 cm<sup>-1</sup>. Calcination of the catalyst samples at 550°C caused some changes in the absorption bands in the low IR region. This result implied that partial aggregation of the Ti species in zeolite cavities might have occurred [24]. This was consistent with the partial drop in the pore volume as observed in the surface analysis.

The FTIR spectra of 0.64 and 1.32 wt.% of La ions loaded on encapsulated titanium are shown in Figure 2(b). No new bands were detected after incorporating La ions into Ti<sub>4</sub>-NaY. However, a small reduction in asymmetric stretching mode of external linkages bond was detected at 1050 cm<sup>-1</sup> after the loading of La ions and this reduction was found to increase with increasing wt.% of La ions. A band at 450 cm<sup>-1</sup> was observed and it was ascribed to T–O stretching vibration mode.

**3.1.5. UV-Vis Spectrophotometer.** The UV-Vis diffuse reflectance spectra for NaY, Ti<sub>4</sub>-NaY, La/Ti<sub>4</sub>-NaY are shown in Figure 3. Blue shifts towards shorter wave lengths about 376 nm were observed for Ti<sub>4</sub>-NaY while the bare TiO<sub>2</sub> (not shown for clearness) had a wave length of about 390 nm. This behavior was in agreement with Easwaramoorthi and Nataraajan [21]. The provenance of such blue shift towards shorter wave length was due to the quantum size effect for semiconductors as the particle size decreased after the modification of TiO<sub>2</sub> into the pores of the zeolite.

The sudden fall in the reflectance at certain particular wave lengths indicated the presence of optical band gap after the ion-exchange of Ti species into zeolite [28]. However, doping of metals into semiconductors can generally reduce its energy gap to cause a shift in the reflection spectra towards higher wavelength. This red shift towards higher wave length

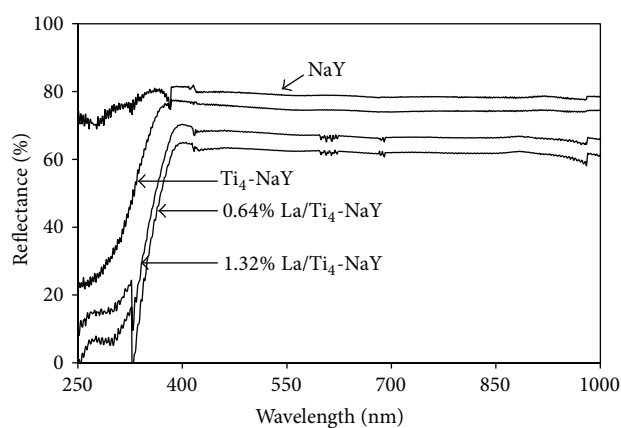


FIGURE 3: The reflection spectra for different samples.

will facilitate the excitation of electron from the valence band to the conduction band. Figure 3 showed that the doping of 0.64 wt.% of La into the Ti<sub>4</sub>-NaY slightly enhances the shift towards higher wave length in comparative to that of Ti<sub>4</sub>-NaY. However, increasing the concentration of La to 1.32 wt.% causes slight blue shift towards shorter wave length. This could be attributed to the difficulties of lanthanum ions to enter the lattice of Ti<sub>4</sub>-NaY at higher concentration instead; it is merely dispersed at the external surface of zeolite and caused this slight enhancement in wavelength shift. Ökte and Yilmaz [3] also observed a decrease in wavelength shift with increasing the La concentration doped in TiO<sub>2</sub>-ZSM-5.

The energy band gap for the samples was calculated from their reflection spectra. There were 3.55 and 3.70 eV for bare TiO<sub>2</sub> and Ti<sub>4</sub>-NaY, respectively. The change in the energy band gap indicated that titanium clusters could have been introduced into the internal pores of zeolite and the sizes of those titanium nanoparticles in the zeolites were smaller than those of bare TiO<sub>2</sub> [17]. However, after the loading of La ions into Ti<sub>4</sub>-NaY, a slight enhancement in the energy gap was observed about 3.60 eV for La/Ti<sub>4</sub>-NaY samples in comparative to that of Ti<sub>4</sub>-NaY.

**3.1.6. EDAX Analysis.** The energy dispersive X-ray (EDX) analysis is an effective technique to provide additional evidence on the success loading of the nanoscale metal on the surface of the support which was not detected in XRD analysis. In Figures 4(a) and 4(b), there were different elements detected on the surface of catalysts such as Si, Al and O which are considered as the main elements of zeolite framework. For instance, at various points in the same sample, different values were obtained at wider range due to the unequal distribution of these elements. Nevertheless, it was believed that the existence of signals attributed to the elements in these samples indicated the success of metals loading during the preparation method.

The EDAX analysis was carried out to verify the success in loading of metal on the surface of the support. Figure 4(a) shows that a small amount of lanthanum was detected on the surface of  $\text{Ti}_4\text{-NaY}$ . On the other hand, Figure 4(b) did not show any signal for the Ti element on the surface of the catalyst. Thus, titanium oxide was successfully encapsulated inside the supercages of the zeolite. According to EDAX analysis, it was clear that titanium was encapsulated into the pores of zeolite and lanthanum nanoparticles agglomerated on the external surface. This conclusion was consistent with results of XRD and UV-Vis reflectance spectra.

**3.1.7. Transmission Electron Microscopy (TEM).** The TEM images were taken for the NaY,  $\text{Ti}_4\text{-NaY}$ , and 0.64%  $\text{La/Ti}_4\text{-NaY}$  catalysts in order to investigate the metal positions for both Ti and La with respect to zeolite structure. Figures 5(a) and 5(b) presents the hexagonal structure of zeolite at two different magnifications 8 k and 45 k, respectively. However, the structure of zeolite remained unchanged after the loading of Ti and La species after the ion-exchange method. In Figures 5(c) and 5(d) at 45 k magnification, there were dark and light spots distinguished at the outside and the inner side of the nanoporous structure. The light spots in Figure 5(c) existed between the lattice plan of zeolite ascribed to  $\text{TiO}_2$  clusters, while the dark spots at the outer edge of the zeolite particle in Figure 5(d) were ascribed to La since the molecular weight of lanthanum is much higher than that of titanium. Thus, the TEM image of the former gave more dark spots than Ti. Due to the overlapping of the metals with the matrix of zeolite, it was rather difficult to measure the diameter of these metals nanoparticles.

**3.1.8. AFM Technique.** The three-dimensional images with a scan area of  $10 \times 10 \mu\text{m}$  for the parent NaY,  $\text{Ti}_4\text{-NaY}$ , and 0.64%  $\text{La/Ti}_4\text{-NaY}$  were carried out using atomic force microscopy AFM technique to investigate the variation in the surface morphology for the prepared samples as presented in Figure 6. The results showed that both NaY and  $\text{Ti}_4\text{-NaY}$  have similar surface characteristic and the roughness value for both catalysts was around 72–74 nm. This insignificant change in roughness value supports the previous characterization results and that the  $\text{TiO}_2$  clusters were encapsulated into the cages of zeolite instead of its surface. However, for the case of 0.64%  $\text{La/Ti}_4\text{-NaY}$  the roughness of the surface was decreased significantly to 44 nm due to the agglomeration of

La oxide on the surface of zeolite. This result was in agreement with the XRD and TEM results.

### 3.2. Sonocatalytic Degradation Process

**3.2.1. Control Experiment.** Before starting the sonocatalytic reaction a preliminary study was carried out to investigate the color removal of Amaranth dye by the catalyst in the absence of ultrasonic irradiation. An aqueous solution of Amaranth with initial dye concentration of 10 mg/L was mixed separately with 1.5 g/L catalyst of  $\text{Ti}_4\text{-NaY}$  and 0.64%  $\text{La/Ti}_4\text{-NaY}$  at ambient temperature for 2 h in the absence of ultrasonic irradiation, and the pH of the dye around 5.6 was kept normal without any prior adjustment. No adsorption was indicated at the surface of the catalysts by using the magnetic stirrer for 2 h as it is shown in Figure 7. On the other hand, the degradation of the Amaranth by ultrasonic alone in the absence of catalyst was 12% only at the same reaction conditions of 10 mg/L of initial dye concentration, normal pH, and a catalyst loading of 1.5 g/L. This low activity of the ultrasonic was ascribed to the insufficient amount of  $\cdot\text{OH}$  radicals generated by ultrasonic alone since radicals in this case were generated only through the dissociation of water molecules. As a result, the oxidation of the hydrophilic dye molecules could be only effective when these radicals were transferred from the interface of the cavitation bubbles into the bulk solution [29]. However, encapsulation of titanium nanoparticles into the pores of zeolite gave significant enhancement in the sonocatalytic activity with maximum degradation efficiency of 50%. Increasing the sonocatalytic activity was completely ascribed to the synergistic between the encapsulated titanium and ultrasonic irradiation since no adsorption ability for the catalyst was detected. The effect of  $\text{TiO}_2$  encapsulated into zeolite results will be discussed in details in the next section.

**3.2.2. Effect of  $\text{TiO}_2$  Amount Encapsulation into NaY.** Sonocatalytic degradation of Amaranth dye with different amounts of titanium incorporated into the sodium zeolite was investigated and the results are as shown in Figure 8. The highest degradation value was 50% with  $\text{Ti}_4\text{-NaY}$  which had the highest titanium loading among the materials tested. Increasing loading of titanium had minimal impact on the active catalytic surface due to the presence of Ti into the supercages in zeolite Y. As such, preference accumulation of titanium in these supercages would render the internal micropores of the zeolites to be virtually unaffected by the nanoparticles [20]. As such, minimal drops in the pore area and volume were demonstrated by the titanium-modified zeolite Y samples. The results also suggested that ultrasonic waves could reach the internal pores through the water medium. This was clearly the superior characteristic of ultrasonication process. Higher number of titanium sites enabled more generation of hydroxyl radicals upon ultrasonic irradiation to improve the degradation efficiency. The presence of the heterogeneous catalyst with the ultrasonic irradiation enhance, the activity of sonocatalytic process due to the effect of mechanical stirring produced by ultrasonic, the mass

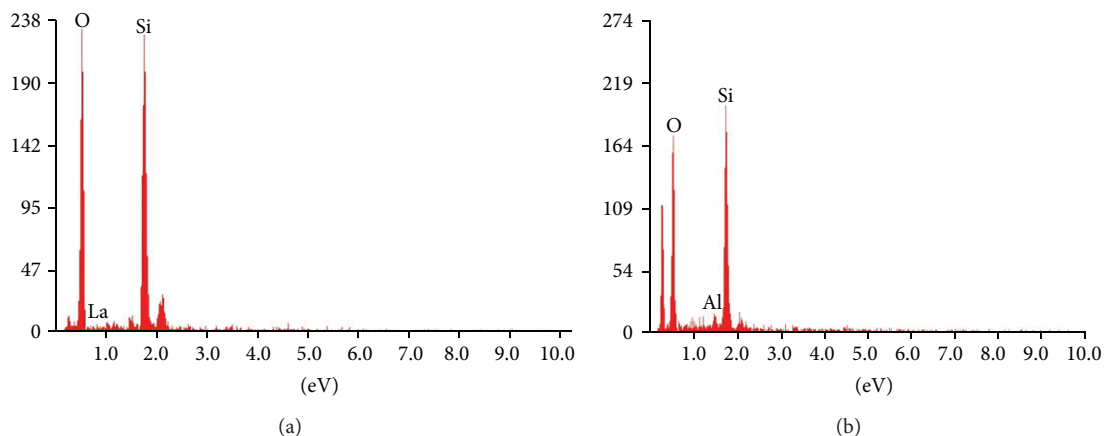


FIGURE 4: EDAX analysis results for (a) 0.64% La/Ti<sub>4</sub>-NaY and (b) Ti<sub>4</sub>-NaY.

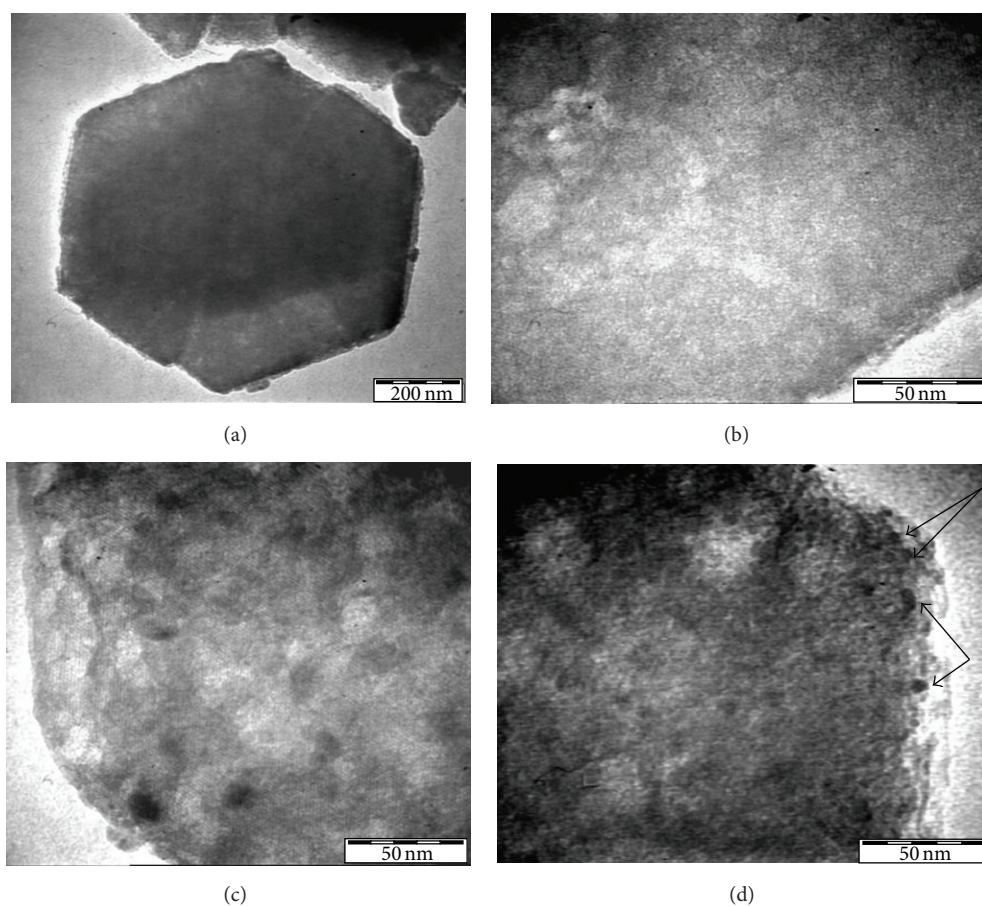


FIGURE 5: TEM images for NaY ((a) and (b)) at 8 k and 45 k magnification, respectively, (c) Ti<sub>4</sub>-NaY, and (d) 0.64% La/Ti<sub>4</sub>-NaY.

transfer, and the activation of the catalyst surface leading to the generation of more reactive nucleation sites which were responsible for the production of more hot spots to enhance the production of free radicals [18].

**3.2.3. Effect of La Loading on Titanium Oxide Encapsulated into NaY.** The catalyst with the highest titanium content that

is, Ti<sub>4</sub>-NaY, was chosen to load the lanthanum nitrate with different loadings, that is, 0.32, 0.64, and 1.28 wt.%, of La in order to investigate the effect of this metal on the sonocatalytic process. Figure 9 shows the degradation of Amaranth during the ultrasonic-assisted reaction at 10 mg/L initial dye concentration, original pH with a catalyst loading of 1.5 g/L for 2 h. No significant enhancement in decolorization efficiency was noticed after the loading of La onto

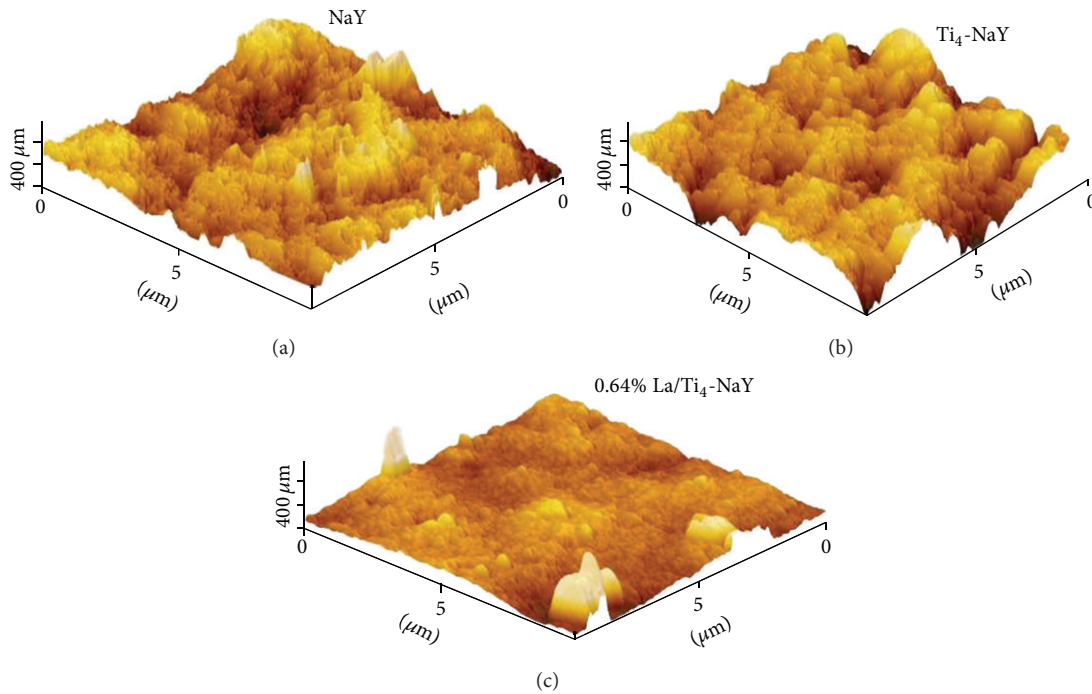


FIGURE 6: AFM 3-dimensional images for different samples.

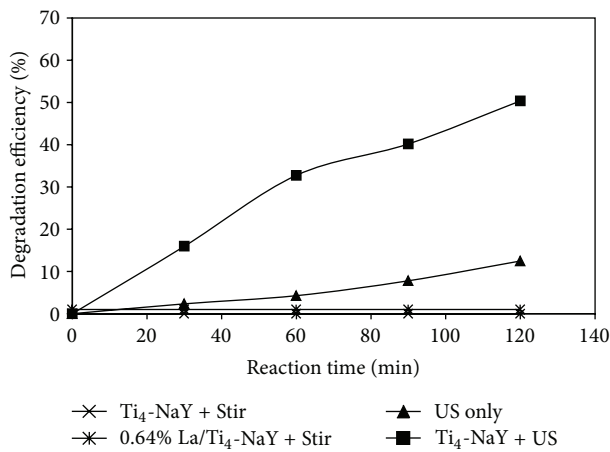


FIGURE 7: Preliminary study of the catalysts with and without ultrasonic irradiation (10 mg/L initial dye solution, 1.5 g/L catalyst loading, original pH, and 120 min of reaction).

Ti<sub>4</sub>-NaY. The catalytic activity with different wt.% La loading was reduced from 50% for Ti<sub>4</sub>-NaY to 33% for 1.28% La/Ti<sub>4</sub>-NaY. This reduction in catalytic activity was associated with the agglomeration of the lanthanum oxide, that is, La<sub>2</sub>O<sub>3</sub> nanoparticles which might be formed after the calcination step mainly on the external surface of the zeolite. Thus the nanoparticles, of La oxide could block the production of TiO<sub>2</sub> clusters and shield the irradiation source from reaching the titanium clusters encapsulated into zeolite. This result was in agreement with the XRD and the AFM results as most of La oxides formed were located at the surface of the Ti<sub>4</sub>-NaY catalyst. Furthermore, with increasing the La loading,

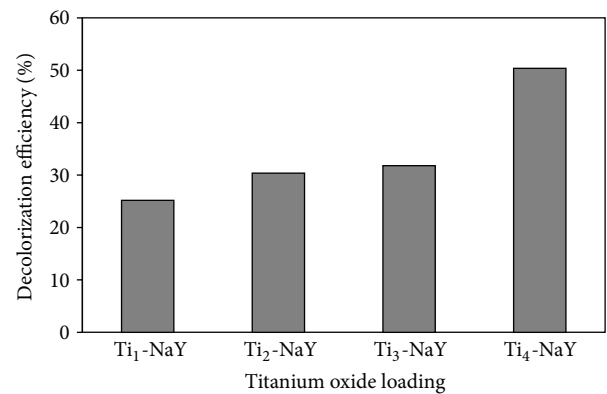


FIGURE 8: Degradation efficiency of Amaranth with different loadings of titanium (initial dye concentration 10 mg/L, catalyst loading 1.5 g/L, original pH, and 120 min of reaction time).

the ability of these ions to separate electron-hole pairs will be reduced. These results can be supported by the results obtained from Uv-Vis analysis since slight enhancement in energy gap was only occurred and further increase in wt.% of La caused a blue shift to lower wave length thus causing more reduction in catalytic activity up to 33%.

Ökte and Yilmaz [3] reported that the loading of La into TiO<sub>2</sub>-ZSM-5 catalyst enhanced the catalytic activity for the degradation of methyl orange dye. However, the locations of the La and TiO<sub>2</sub> were both at the surface of ZSM-5. Inversely, the present work is dealing with the effect of La loading with titanium encapsulated into zeolite. The differences in the characteristics of the catalysts produced in this work



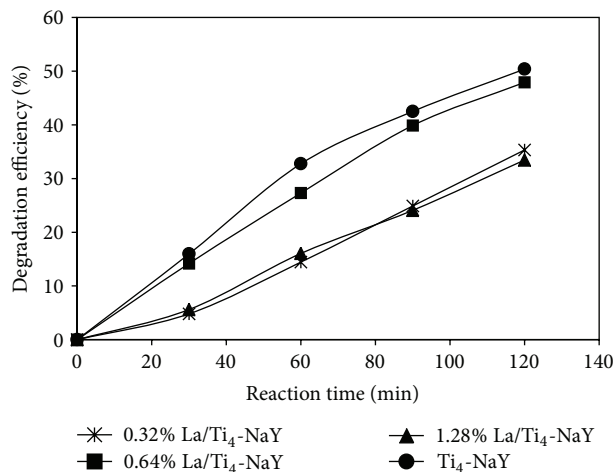


FIGURE 9: Degradation of Amaranth for Ti<sub>4</sub>-NaY catalysts with different loadings of lanthanum (10 mg/L initial dye solution, catalyst loading 1.5 g/L, and original pH).

were ascribed to the metal incorporation procedures and its location with respect to zeolite structure. Our earlier work [30] successfully synthesized the Fe loaded on TiO<sub>2</sub> encapsulated into zeolite and it was confirmed to be a promising catalyst due to its high decolorization efficiency. The Fe ions were able to enter the lattice of Ti<sub>4</sub>-NaY due to the smaller size of Fe<sup>3+</sup> in comparative to that of La<sup>3+</sup> and cause a significant reduction in the energy gap of the produced catalyst up to 2.8 eV at loading of 0.8 wt.% of Fe ion. As such, important factors should be considered to get best catalytic activity, that is, selection of the suitable preparation method selection of the suitable dopant metal bearing in mind the ionic radius of the metal and the pore size of the support.

#### 4. Conclusions

Different amounts of titanium were successfully encapsulated inside the cages of Y zeolite using ion-exchange method. Characterization results suggested that the structure of zeolite remained virtually unchanged after the encapsulation. There was no titanium atom observed on the surface of the zeolite catalyst according to the EDAX and AFM analyses to suggest the successful incorporation within the internal pores. The UV-Vis spectrum for Ti-NaY demonstrated blue shifts towards short wave lengths while a slight red shift was detected after the loading of 0.64% La into Ti<sub>4</sub>-NaY. The maximum degradation efficiency of Amaranth in 2 h was 50% and it was observed with the highest titanium amount loading in Ti<sub>4</sub>-NaY. The encapsulated titanium into zeolite improved the activity of the zeolite catalyst in the sonocatalytic process owing to the ability of the ultrasound to penetrate into the micro- or mesoporous supports that improved the generation of the radicals by the TiO<sub>2</sub> located within the zeolite host. On the other hand, the activity of the catalyst decreased after the doping with lanthanum. This reduction in catalytic activity was ascribed to the poor contact between the metal that was mostly existed at the external surface of the catalyst and

the titanium nanoparticles that were encapsulated into the supercages of zeolite.

#### Acknowledgment

The Research University grant from Universiti Sains Malaysia to support this work is gratefully acknowledged.

#### References

- [1] V. K. Gupta, R. Jain, A. Mittal, M. Mathur, and S. Sikarwar, "Photochemical degradation of the hazardous dye Safranin-T using TiO<sub>2</sub> catalyst," *Journal of Colloid and Interface Science*, vol. 309, no. 2, pp. 464–469, 2007.
- [2] S. Yamaguchi, T. Fukura, Y. Imai, H. Yamaura, and H. Yahiro, "Photocatalytic activities for partial oxidation of  $\alpha$ -methylstyrene over zeolite-supported titanium dioxide and the influence of water addition to reaction solvent," *Electrochimica Acta*, vol. 55, no. 26, pp. 7745–7750, 2010.
- [3] A. N. Ökte and Ö. Yılmaz, "La and Ce loaded TiO<sub>2</sub>-ZSM-5 catalysts: comparative characterization and photocatalytic activity investigations," *Microporous and Mesoporous Materials*, vol. 126, no. 3, pp. 245–252, 2009.
- [4] L. Song, C. Chen, S. Zhang, and Q. Wei, "Sonocatalytic degradation of amaranth catalyzed by La<sup>3+</sup> doped TiO<sub>2</sub> under ultrasonic irradiation," *Ultrasonics Sonochemistry*, vol. 18, no. 5, pp. 1057–1061, 2011.
- [5] N. A. Jamalluddin and A. Z. Abdullah, "Reactive dye degradation by combined Fe(III)/TiO<sub>2</sub> catalyst and ultrasonic irradiation: effect of Fe(III) loading and calcination temperature," *Ultrasonics Sonochemistry*, vol. 18, no. 2, pp. 669–678, 2011.
- [6] J. Wang, Y. Lv, Z. Zhang et al., "Sonocatalytic degradation of azo fuchsin in the presence of the Co-doped and Cr-doped mixed crystal TiO<sub>2</sub> powders and comparison of their sonocatalytic activities," *Journal of Hazardous Materials*, vol. 170, no. 1, pp. 398–404, 2009.
- [7] Y. Zhang, S. Deng, B. Sun et al., "Preparation of TiO<sub>2</sub>-loaded activated carbon fiber hybrids and application in a pulsed discharge reactor for decomposition of methyl orange," *Journal of Colloid and Interface Science*, vol. 347, no. 2, pp. 260–266, 2010.
- [8] S. Sampath, H. Uchida, and H. Yoneyama, "Photocatalytic degradation of gaseous pyridine over zeolite-supported titanium dioxide," *Journal of Catalysis*, vol. 149, no. 1, pp. 189–194, 1994.
- [9] K. Hofstadler, R. Bauer, S. Novalic, and G. Heisler, "New reactor design for photocatalytic wastewater treatment with TiO<sub>2</sub> immobilized on fused-silica glass fibers: photomineralization of 4-chlorophenol," *Environmental Science Technology*, vol. 28, no. 4, pp. 670–674, 1994.
- [10] H. Yoneyama, S. Haga, and S. Yamanaka, "Photocatalytic activities of microcrystalline TiO<sub>2</sub> incorporated in sheet silicates of clay," *The Journal of Physical Chemistry*, vol. 93, pp. 4833–4837, 1989.
- [11] X. Liu, K.-K. Iu, and J. K. Thomas, "Preparation, characterization and photoreactivity of titanium(IV) oxide encapsulated in zeolites," *Journal of the Chemical Society, Faraday Transactions*, vol. 89, no. 11, pp. 1861–1865, 1993.
- [12] M. Abd El-Moteleb, A. M. A. Hassan, T. A. Ibrahim, M. Abdelbaset, and S. Hassaan, "Photocatalytic degradation of some dyes using La/Ti/ZSM-5," *Assut University Environment Research*, vol. 12, no. 2, pp. 9–21, 2009.

- [13] S. M. Drechsel, R. C. K. Kaminski, S. Nakagaki, and F. Wypych, "Encapsulation of Fe(III) and Cu(II) complexes in NaY zeolite," *Journal of Colloid and Interface Science*, vol. 277, no. 1, pp. 138–145, 2004.
- [14] A. Pourahmad and S. Sohrabnezhad, "A cost effective and sensitive method for the determination of ammonia concentration in nanocrystal mordenite," *International Journal of Nano Dimension*, vol. 1, pp. 143–152, 2010.
- [15] X. Liu, K.-K. Iu, and J. Kerry Thomas, "Encapsulation of TiO<sub>2</sub> in zeolite Y," *Chemical Physics Letters*, vol. 195, no. 2-3, pp. 163–168, 1992.
- [16] H. Chen, A. Matsumoto, N. Nishimiya, and K. Tsutsumi, "Preparation and characterization of TiO<sub>2</sub> incorporated Y-zeolite," *Colloids and Surfaces A*, vol. 157, no. 1–3, pp. 295–305, 1999.
- [17] G. Zhang, W. Choi, S. H. Kim, and S. B. Hong, "Selective photocatalytic degradation of aquatic pollutants by titania encapsulated into FAU-type zeolites," *Journal of Hazardous Materials*, vol. 188, no. 1–3, pp. 198–205, 2011.
- [18] Y. L. Pang, S. Bhatia, and A. Z. Abdullah, "Process behavior of TiO<sub>2</sub> nanotube-enhanced sonocatalytic degradation of Rhodamine B in aqueous solution," *Separation and Purification Technology*, vol. 77, no. 3, pp. 331–338, 2011.
- [19] R. J. Tayade, R. G. Kulkarni, and R. V. Jasra, "Enhanced photocatalytic activity of TiO<sub>2</sub>-Coated NaY and HY zeolites for the degradation of methylene blue in water," *Industrial and Engineering Chemistry Research*, vol. 46, no. 2, pp. 369–376, 2007.
- [20] C.-C. Wang, C.-K. Lee, M.-D. Lyu, and L.-C. Juang, "Photocatalytic degradation of C.I. Basic Violet 10 using TiO<sub>2</sub> catalysts supported by Y zeolite: an investigation of the effects of operational parameters," *Dyes and Pigments*, vol. 76, no. 3, pp. 817–824, 2008.
- [21] S. Easwaramoorthi and P. Natarajan, "Photophysical properties of phenosafranin (PHNS) adsorbed on the TiO<sub>2</sub>-incorporated zeolite-Y," *Microporous and Mesoporous Materials*, vol. 86, no. 1–3, pp. 185–190, 2005.
- [22] X. S. Zhao, G. Q. Lu, and G. J. Millar, "Encapsulation of transition metal species into zeolites and molecular sieves as redox catalysts: part I—preparation and characterisation of nanosized TiO<sub>2</sub>, CdO and ZnO semiconductor particles anchored in NaY zeolite," *Journal of Porous Materials*, vol. 3, no. 1, pp. 61–66, 1996.
- [23] R. Castillo, B. Koch, P. Ruiz, and B. Delmon, "Influence of the amount of titania on the texture and structure of titania supported on silica," *Journal of Catalysis*, vol. 161, no. 2, pp. 524–529, 1996.
- [24] S. Anandan and M. Yoon, "Photocatalytic activities of the nanosized TiO<sub>2</sub>-supported Y-zeolites," *Journal of Photochemistry and Photobiology C*, vol. 4, no. 1, pp. 5–18, 2003.
- [25] L. P. Xu, Y. X. Zhao, Z. G. Wu, and D. S. Liu, "A new method for preparing Ti-Si mixed oxides," *Chinese Chemical Letters*, vol. 14, no. 11, pp. 1159–1162, 2003.
- [26] Y. Kim and M. Yoon, "TiO<sub>2</sub>/Y-zeolite encapsulating intramolecular charge transfer molecules: a new photocatalyst for photoreduction of methyl orange in aqueous medium," *Journal of Molecular Catalysis A*, vol. 168, no. 1-2, pp. 257–263, 2001.
- [27] H. Hassan and B. H. Hameed, "Oxidative decolorization of Acid Red 1 solutions by Fe-zeolite Y type catalyst," *Desalination*, vol. 276, no. 1–3, pp. 45–52, 2011.
- [28] G. P. Joshi, N. S. Saxena, T. P. Sharma, and S. C. K. Mishra, "Measurement of thermal transport and optical properties of conducting polyaniline," *Indian Journal of Pure and Applied Physics*, vol. 44, no. 10, pp. 786–790, 2006.
- [29] S. Meshram, D. Tayade, P. Ingle, P. D. Jolhe, B. Diwate, and S. Biswas, "Ultrasonic cavitation induced degradation of Congo red in aqueous solutions," *Chemical Engineering Research Bulletin*, vol. 14, pp. 119–123, 2010.
- [30] A. H. Alwash, A. Z. Abdullah, and N. Ismail, "Zeolite Y encapsulated with Fe-TiO<sub>2</sub> for ultrasound-assisted degradation of amaranth dye in water," *Journal of Hazardous Materials*, vol. 233-234, pp. 184–193, 2012.



**Hindawi**

Submit your manuscripts at  
<http://www.hindawi.com>

